Biochemical Characterization and Structural Analysis of a Highly Proficient Cocaine Esterase[†,‡]

James M. Turner,[§,||] Nicholas A. Larsen,[§,||] Amrik Basran,[⊥] Carlos F. Barbas, III,[§,||] Neil C. Bruce,[⊥] Ian A. Wilson,*[,§,||] and Richard A. Lerner*[,§,||]

Department of Molecular Biology, The Scripps Research Institute, 10550 North Torrey Pines Road, La Jolla, California 92037, The Skaggs Institute for Chemical Biology, The Scripps Research Institute, 10550 North Torrey Pines Road, La Jolla, California 92037, and Institute of Biotechnology, Cambridge University, Tennis Court Road, Cambridge CB2 1QT, U.K.

Received May 15, 2002; Revised Manuscript Received August 1, 2002

ABSTRACT: The bacterial cocaine esterase, cocE, hydrolyzes cocaine faster than any other reported cocaine esterase. Hydrolysis of the cocaine benzoyl ester follows Michaelis−Menten kinetics with $k_{cat} = 7.8\ s^{-1}$ and $K_M = 640$ nM. A similar rate is observed for hydrolysis of cocaethylene, a more potent cocaine metabolite that has been observed in patients who concurrently abuse cocaine and alcohol. The high catalytic proficiency, lack of observable product inhibition, and ability to hydrolyze both cocaine and cocaethylene make cocE an attractive candidate for rapid cocaine detoxification in an emergency setting. Recently, we determined the crystal structure of this enzyme, and showed that it is a serine carboxylesterase, with a catalytic triad formed by S117, H287, and D259 within a hydrophobic active site, and an oxyanion hole formed by the backbone amide of Y118 and the Y44 hydroxyl. The only enzyme previously known to use a Tyr side chain to form the oxyanion hole is prolyl oligopeptidase, but the Y44F mutation of cocE has a more deleterious effect on the specificity rate constant (k_{cat}/K_M) than the analogous Y473F mutation of prolyl oligopeptidase. Kinetic studies on a series of cocE mutants both validate the proposed mechanism, and reveal the relative contributions of active site residues toward substrate recognition and catalysis. Inspired by the anionic binding pocket of the cocaine binding antibody GNC92H2, we found that a Q55E mutation within the active site of cocE results in a modest (2-fold) improvement in K_M, but a 14-fold loss of k_{cat}. The pH rate profile of cocE was fit to the ionization of two groups ($pK_{a1} = 7.7$; $pK_{a2} = 10.4$) that likely represent titration of H287 and Y44, respectively. We also describe the crystal structures of both S117A and Y44F mutants of cocE. Finally, urea denaturation studies of cocE by fluorescence and circular dichroism show two unfolding transitions (0.5−0.6 M and 3.2−3.7 M urea), with the first transition likely representing pertubation of the active site.

Cocaine is a powerful stimulant and among the most addictive of drugs. The strong reinforcing properties of this drug are explained, in part, by the dopamine hypothesis (*1*). Cocaine blocks the dopamine re-uptake pathway, leading to excess dopamine stimulation in the pleasure center of the brain. According to a National Institute on Drug Abuse research report, in 1997 there were 1.5 million current cocaine users in the United States. In addition, the Substance and Mental Health Services Administration estimated the number of emergency room incidents related to cocaine in 1997 was 161 000. Unfortunately, there is no effective treatment for cocaine overdose, which can result in heart attacks, seizures, and death (*2*−*3*).

The short serum half-life of (−)-cocaine (∼40 min) (*4*−*7*) is mainly due to formation of nonpsychoactive metabolites by enzyme-catalyzed ester hydrolysis. Serum butyrylcholinesterase (BchE)[1] and the liver carboxylesterase hCE-2 hydrolyze the benzoyl ester of (−)-cocaine (**1**) to ecgonine methyl ester (**2**) and benzoic acid (*8*−*10*) (Figure 1, path A). Liver carboxylesterase hCE-1 hydrolyzes the methyl ester of (−)-cocaine (**1**) to yield benzoylecgonine (**3**) and methanol (*11*−*12*) (Figure 1, path B). When (−)-cocaine and alcohol are abused concurrently, a transesterification reaction occurs, which converts (−)-cocaine (**1**) into cocaethylene (**4**) (Figure 1, path C), which has both increased toxicity and lengthened serum half-life (*13*−*15*).

[†] Support was provided by the National Institutes of Health (I.A.W., GM-38273), (R.A.L., CA-27489), and the Biotechnology and Biological Sciences Research Council (N.C.B.). We thank the Howard Hughes Medical Institute (J.M.T.) and the Bernie Gilula Foundation (N.A.L.) for predoctoral fellowships.

[‡] The atomic coordinates and structure factors for the S117A and Y44F mutants have been deposited in the RCSB Protein Data Bank with accession codes 1L7Q and 1L7R, respectively.

* To whom correspondence should be addressed. R. A. L. (Phone: (858) 784-8265. Fax: (858) 784-9899 E-mail: rlerner@scripps.edu.). I. A. W. (Phone (858) 784-9706. Fax: (858) 784-2980. E-mail: wilson@scripps.edu.).

[§] Department of Molecular Biology.

[||] The Skaggs Institute for Chemical Biology.

[⊥] Institute of Biotechnology.

[1] Abbreviations: cocE, cocaine esterase; BchE, butyrylcholinesterase; hCE, human liver carboxylesterase; DOM, domain; DTT, dithiothreitol; IPTG, isopropyl-β-D-thiogalactopyranoside; PBS, phosphate buffered saline; bis-tris propane, 1,3-bis[tris(hydroxymethyl)methylamino]-propane; CAPS, 3-(cyclohexylamino)-1-propanesulfonic acid; vdw, van der Waals.

10.1021/bi026131p CCC: $22.00
Published on Web 09/20/2002

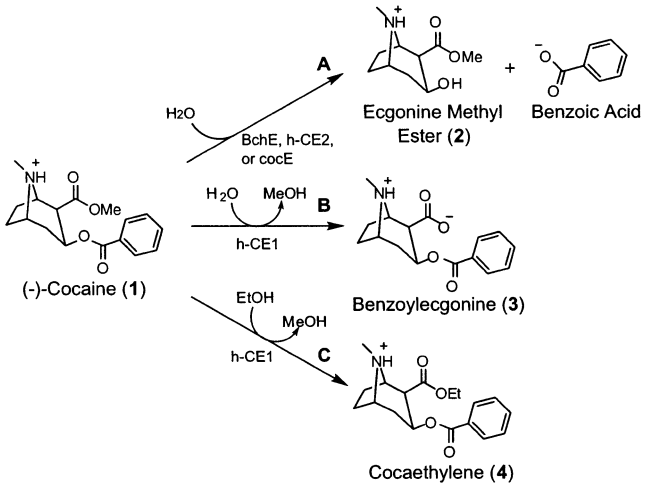

FIGURE 1: Cocaine metabolism by naturally occurring enzymes. (**A**) The benzoyl ester of (−)-cocaine (**1**) is hydrolyzed by butyrylcholinesterase (BchE), human liver carboxylesterase h-CE2, and cocaine esterase (cocE) to egconine methyl ester (**2**) and benzoic acid. (**B**) Human liver carboxylesterase h-CE1 catalyzes the hydrolysis of the methyl ester of (−)-cocaine to benzoylecgonine (**3**). (**C**) When (−)-cocaine and alcohol are concurrently used, an h-CE1-catalyzed transesterification converts (−)-cocaine into cocaethylene (**4**).

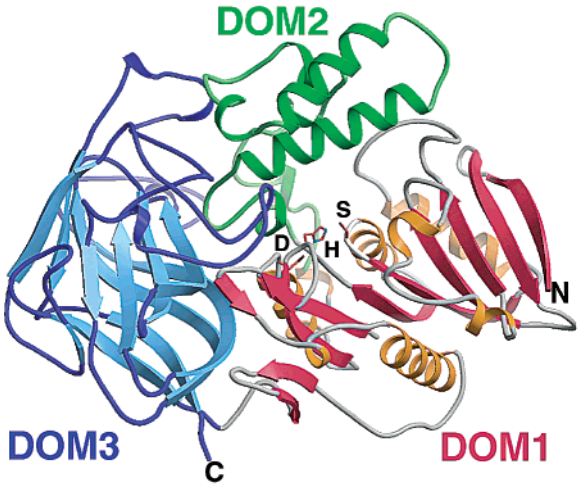

FIGURE 2: Ribbon diagram of the cocE structure. The enzyme is composed of three domains: DOM1 (red β-sheet, orange α-helices, and gray loops), DOM2 (green), and DOM3 (blue). The active site is located at the interface of all three domains, and the residues of the catalytic triad are indicated the letters **S** (S117), **H** (H287), and **D** (D259). Adapted from ref 26.

An attractive mechanism for treatment for acute cocaine overdose is to prevent cocaine from reaching the receptors of action in the brain, such as the dopamine transporter. Research has focused on either the use of cocaine agonists or antagonists (*16*−*17*), administration of a therapeutic protein that hydrolyzes cocaine (*18*), or immunization by a cocaine binding or hydrolyzing antibody (*19*−*22*). Although enzymatic hydrolysis of either the methyl or benzoyl ester of cocaine would be able to provide clearance, hydrolysis of the methyl ester would likely cause the transesterification of cocaine into cocaethylene in patients who concurrently use both cocaine and alcohol. In contrast, hydrolysis of the benzoyl ester of cocaine does not have this potential side effect.

While attempts to develop cocaine agonists have been largely unsuccessful (*16*−*17*), initial experiments have shown that active or passive immunization with a cocaine binding antibody reduces the effects of cocaine (*22*, *23*). While a cocaine binding antibody would effectively reduce the cocaine levels in the brain, the drug concentration in acute overdose patients may exceed the serum antibody concentration. In this case, a therapy based on catalytic breakdown of cocaine would be necessary.

The specificity rate constants (k_{cat}/K_M) of several human esterases, such as hCE-1, hCE-2, and BchE, for cocaine hydrolysis are several orders of magnitude below a diffusion-limited rate (*8*−*12*). These enzymes have not evolved under selection pressure for cocaine hydrolysis, but rather, serendipitously accept cocaine as part of a broad range of substrates. For example, BchE hydrolyzes the nonpharmacologically active (+)-enantiomer of cocaine over 2000 times faster than the naturally occurring (−)-enantiomer (*24*). An enzyme that evolved for cocaine hydrolysis would likely have a faster rate than esterases such as hCE-1, hCE-2, and BchE. If so, this enzyme would also be a useful model system for the study of enzyme-catalyzed cocaine hydrolysis, which may aid in both the improvement of current cocaine catalytic antibodies and the design of haptens to elicit cocaine esterase catalytic antibodies with improved activity.

We have described both the isolation (*25*) and structure determination (*26*) of a cocaine esterase (cocE) from a *Rhodococcal* strain (MB1) that grows in the rhizosphere soil of the cocaine producing plant *Erythroxylum coca*. This enzyme catalyzes hydrolysis of the benzoyl ester of cocaine as the first step in a metabolic pathway that is capable of utilizing cocaine as a sole source of carbon and nitrogen (*25*). CocE is one of only two known enzymes that are believed to have evolved under selection pressure for cocaine hydrolysis (*27*), and we considered it likely that this enzyme would be much more proficient at cocaine hydrolysis than other esterases such as BchE, hCE-1, and hCE-2.

The crystal structure of cocE (*26*) revealed a globular enzyme composed of three domains (DOM1, DOM2, and DOM3) (Figure 2). The enzyme is a member of the α/β hydrolase superfamily (*28*, *29*), with a hydrophobic active site located at the interface of all three domains. Within the active site is a prototypical catalytic triad formed by S117, H287, and D259 (Figure 2). We have also previously described crystal structures of cocE bound to benzoate, a product of the cocaine hydrolysis reaction and bound to phenyl boronic acid, an analogue of the tetrahedral intermediate (*26*).

The negatively charged tetrahedral intermediate that is formed in the mechanism of serine hydrolases is stabilized through interactions with the oxyanion hole of the enzyme (*30*−*32*). Different classes of esterases and proteases use different motifs in formation of the oxyanion hole. For example, in the chymotrypsin class of enzymes, the oxyanion hole is formed by the backbone NH groups of the catalytic S195 and G193 (*32*), while acetylcholinesterase and members of the hormone-sensitive lipase subfamily use three backbone NH groups to form the oxyanion hole (*33*, *34*). In addition to backbone amides, some serine hydrolases employ side chains to form the oxyanion hole. For example, the subtilisin-type enzymes substitute a side-chain amide of asparagine for a main-chain NH (*32*). The crystal structure of cocE revealed that the oxyanion hole of cocE is formed by the

hydroxyl of Y44 and the backbone amide of Y118, adjacent to the catalytic S117 (*26*). The only other known esterase that uses a Tyr hydroxyl to form the oxyanion hole is prolyl oligopeptidase, which uses the hydroxyl of Y473 and the main-chain NH of N555, adjacent to the catalytic serine, S554 (*31, 32*).

Herein, we report biochemical and structural studies on cocE. Kinetics of both wild-type and mutant enzymes, as well as a pH-rate profile of the wild-type enzyme, reveal the relative contribution of active site residues for substrate recognition, and support the binding model based on the crystal structure. We also describe the crystal structures of the S117A and Y44F mutants of cocE, as well as urea unfolding studies on the wild-type, S117A, and Y44F mutant enzymes. This structural and biochemical information about cocE both provides some explanation for the improved catalytic activity of cocE over other esterases and cocaine catalytic antibodies, and allows comparisons to be made between cocE, prolyl oligopeptidase, and the cocaine binding antibody GNC92H2 (*23, 35*).

MATERIALS AND METHODS

Cloning and Protein Expression. Luria broth and agar were obtained from Life Technologies (Gaithersburg, MD). The cocE enzyme was subcloned into pET-22b(+) (Novagen) and transformed into BL21-Gold (DE3) cells (Stratagene). Soluble enzyme (20 mg L^{-1}) was obtained by overnight induction with 1mM isopropyl-β-D-thiogalactopyranoside (IPTG) at ~23 °C. CocE was ~99% pure after two consecutive rounds of Ni−NTA agarose chromatography (Qiagen).

Crystallization, Structure Solution, and Refinement of Y44F and S117A cocE mutants. The Y44F and S117A mutants were expressed and crystallized as reported **(***26***)**. In brief, the soluble *E. coli* lysate was purified by Ni-agarose chromatography, dialyzed against PBS (4 × 2 L), and against Ni-agarose binding buffer (2 × 2 L) (Qiagen), purified again by Ni-agarose chromatography, dialyzed into 10mM Tris pH 7.5, 25 mM NaCl, 5mM DTT, and concentrated to 25 mg mL^{-1}. The enzyme was ~99% pure as determined by gel electrophoresis stained with Coomassie blue. Crystals were grown from 1.4 to 1.6 M ammonium sulfate in space group *P*6522, with a = *b* = 106 Å, and *c* = 220 Å. Data were collected at the Stanford Synchotron Radiation Laboratory (SSRL), beamlines 9-2 (Y44F mutant) and 11-1 (S117A mutant), and processed with HKL2000 (*36*) (Table 1). The mutant structures were refined in CNS (*37*) using the native enzyme structure as a starting model (PDB 1JU4). The final statistics were R_{cryst} = 19.0%, R_{free} = 21.0%, and R_{cryst} = 18.3%, and R_{free} = 20.4% for the Y44F and S117A mutants, respectively (Table 1). Only three portions of the molecule contain notable disorder, including the amino and carboxyl termini, and a loop region that connects helices H2 and H3 in domain 2 (DOM2). This disordered loop consists of residues 178−180 and residues 175−181 in the Y44F and S117A structures, respectively. Two additional *N*-terminal residues were refined in the Y44F mutant, which were not visible in the S117A mutant or in the previously determined wild-type complexes.

Mutagenesis. Standard desalted primers for mutagenesis were purchased from Retrogen (San Diego, CA). All mutagenesis was done with the QuickChange site-directed mutagenesis kit (Stratagene, La Jolla, CA). The primers used for mutagenesis are listed below. Bold font corresponds to the codon that was mutated. (Y44F) 5′ sense cgcaaccca**ttc**gacaagttcg, 5′ antisense cgaacttgtc**gaa**tgggttgcg; (Q55A) 5′ sense gttcgcgtggtcgacg**gcg**tcgacaaactggcttg, 5′ antisense caagccagtttgtcga**cgc**cgtcgaccacgcgaac; (Q55E) 5′ sense cgtggtcgacg**gag**tcgacaaactg, 5′ antisense cagtttgtcga**ctc**cgtcgaccacg; (S117A) 5′ sense gttcggcgtt**gcg**tacttgggtg, 5′ antisense caccaagta**cgc**aacgccgaac; (S117C) 5′ sense gtgggcatgttcggcgtt**tgc**tacttgggtgtgacc, 5′ antisense ggtcacacccaagta**gca**aacgccgaacatgcccac; (W151A) 5′ sense ccgcgccccg**gcg**tacggccctgg, 5′ antisense ccagggccgta**cgc**cggggcgcgg; (W166A) 5′ sense gctgttgggc**gcg**tcagctctcatag, 5′ antisense ctatgagagctga**cgc**gccaacagc; (D259N) 5′ sense gctgggtggtac**aac**gggttcgtcg, 5′ antisense cgacgaaccc**gtt**gtaccacccagc; (F261A) 5′ sense ggtacgacggg**gcg**gtcggcgaatc, 5′ antisense gattcgccgac**cgc**cccgtcgtacc; (H287A) 5′ sense gcccttggagt**gcc**agcaacctcac, 5′ antisense gtgaggttgct**ggc**actccaagggc; (L407A) 5′ sense ctcgggggacgctg**gcg**ttccacaacggagac, 5′ antisense gtctccgttgtggaa**cgc**cagcgtccccccgag; (F408A) 5′ sense ctcgggggacgctgctg**gcc**cacaacggagacaacg, 5′ antisense cgttgtctccgttgtg**ggc**cagcagcgtccccccgag. The desired mutation was confirmed by DNA sequencing at the Protein and Nucleic Acids Core Facility of The Scripps Research Institute.

Table 1: Data Collection and Refinement Statistics for the S117A and Y44F CocE Mutant Crystal Structures

	Data Collection S117A mutant	Y44F mutant
wavelength (Å)	0.97 (SSRL 11-1)	1.08 (SSRL 9-2)
resolution range (Å)[a]	30−1.76 (1.79−1.76)	30−1.64 (1.67−1.64)
no. of unique refs	74 054	91 569
completeness (%)	98.9 (98.1)	97.1 (74.4)
redundancy	3.5 (3.6)	6.3 (1.8)
R_{merge}[b]	5.4 (49.4)	4.8 (44.8)
I/σ	19.4 (2.5)	39.1 (1.8)

	Refinement Statistics S117A mutant	Y44F mutant
refined residues	571	573
refined waters	583	592
R_{cryst}[c]	18.3%	19.0%
R_{free}[d]	20.4%	21.0%
average *B* values (Å^2)		
enzyme	23.6	21.6
waters	34.0	32.3
ligand	23.5	n/a
Ramachandran statistics		
most favored	86.0%	87.2%
additional allowed	12.2%	11.3%
generously allowed	1.0%	0.6%
disallowed	0.8%	0.8%
deviations from ideal geometry (RMS)		
bond lengths	0.005 Å	0.007 Å
bond angles	1.35°	1.43°
dihedral angles	24.3°	24.6°
improper angles	0.81°	0.90°

[a] Values in parentheses refer to the highest resolution shell. [b] $R_{merge} = [\Sigma_h\Sigma_i\ |I_i(h) - \langle I(h)\rangle|/\Sigma_h\Sigma_i I_i(h)]100$, where $\langle I(h)\rangle$ is the average intensity of *i* symmetry related observations of reflections with Bragg index *h*. [c] $R_{cryst} = [\Sigma_{hkl}\ |F_o - F_c|/\Sigma_{hkl}\ |F_o|\ ]100$, where F_o and F_c are the observed and calculated structure factors. [d] R_{free} was calculated as for R_{cryst}, but on 5% of data excluded before refinement.

Kinetic Measurements. Cocaine and cocaethylene were purchased from Sigma-Aldrich Corp (St. Louis, MO). Wild-type and mutant enzyme concentrations were determined using the Coomassie Plus Protein Assay Reagent Kit (Pierce) with bovine serum albumin (Pierce) as a standard. Initial rates were determined by following the change in absorbance at 240 nm (*8*) in a SpectraMax Plus 384 UV plate reader (Molecular Devices) using SOFTmax Pro software (Version 3.1.2). The reaction was initiated by adding 150 μL of a 2× enzyme solution to 150 μL of a 2× cocaine solution. Final enzyme concentrations ranged from 50 μg mL^{-1} to 50 ng mL^{-1}. Final cocaine concentrations were as follows: 125, 62.5, 31.25, 15.63, 7.81, 3.91, 1.95, and 0.977 μM. For the kinetics of the wild-type and mutant cocE, the buffer was phosphate buffered saline (PBS) pH 7.4. For the pH rate profile, a buffer of 50mM bis-tris propane, 50 mM CAPS, and 100 mM NaCl was used, adjusted to the following pH values with HCl or NaOH: 6.5, 7.3, 7.7, 8.1, 8.5, 8.9, 9.3, 9.7, 10.1, and 10.5. Initial rates were fit to the Michaelis−Menten equation, with k_{cat} and K_M as adjustable parameters (Kaleidagraph 3.0.5, Abelbeck Software). Each reported value of k_{cat} and K_M represents the mean of at least three independent measurements, with the exception of the pH dependence studies, which represent the mean of two independent measurements. Reported errors are the standard deviation of the values measured. The pH dependence of k_{cat} was fit using equation **1** (*31*), with k_{max}, pK_{a1}, and pK_{a2} as adjustable parameters. The K_M and k_{cat}/K_M pH-dependent graphs were plotted using a smooth fitting function (Kaleidagraph V 3.0.5).

$$k_{cat}(\mathrm{pH}) = k_{max}(1 + 10^{\mathrm{pK_{a1}-pH}} + 10^{\mathrm{pH-pK_{a2}}})^{-1} \quad (1)$$

Urea Denaturation. For measurements by fluorescence, the enzyme in PBS was added to urea buffer in PBS to a final enzyme concentration of 1.5 μM (1 mL final reaction volume), and allowed to equilibrate overnight at 23°C. Fluorescence (Em_{obs}) ($\lambda_{ex} = 280$; $\lambda_{em} = 320$) was measured at room temperature using a SpectraMAX Gemini spectrofluorometer plate reader (Molecular Devices), with background subtracted (*38*). Each data point is the mean of four independent measurements. The data were normalized and fit to a double sigmoidal plot (eq **2**) by minimizing the difference between Em_{fit} and Em_{obs}, with Em_{min}, $Em_{intermediate}$, Em_{max}, $[urea]_1$, $[urea]_2$, n_1, and n_2 as the adjustable parameters. $[urea]_1$ and $[urea]_2$ are the urea concentrations at the first and second transitions, respectively, and n_1 and n_2 are measurements of the cooperativity of the transitions.

$$Em_{fit} = Em_{min} + \frac{Em_{intermediate} - Em_{min}}{1 + 10^{n_1([urea]_1 - [urea])}} + \frac{Em_{min} - Em_{intermediate}}{1 + 10^{n_2([urea]_2 - [urea])}} \quad (2)$$

Samples for circular dichroism (CD) measurements were similarly prepared, except that the final protein concentration was 7μM. Full CD spectra were collected on an AVIV 60DS spectropolarimeter, equipped with a temperature-controlled cell holder. Each sample was aliquoted in a 0.1 cm quartz cuvette, and spectra were collected from 210 to 260 nm with a 1 s time constant and step size of 0.5 nm (*38*). The molar ellipticity at 222 nm was calculated from $[\Theta_{222}] = \Theta(10 \times \mathrm{lcn})^{-1}$, where Θ are the raw data in millidegrees, l is the cell path length in cm, c is the molar concentration of enzyme, and n is the number of amino acids. Data were also normalized and fit to a double sigmoidal plot.

Table 2: Kinetics of Cocaine Hydrolysis by Wild-Type and Mutant CocE

CocE mutant	k_{cat} (s^{-1})	K_M (μM)	k_{cat}/K_M (s^{-1} M^{-1})
wild-type	7.8 (±0.1)	0.64 (±0.02)	1.2 (±0.04) × 10^7
wild-type with **4**	9.4 (±0.2)	1.6 (±0.1)	5.9 (±0.4) × 10^6
F261A	0.27 (±0.02)	9.6 (±0.9)	2.8 (±0.3) × 10^4
W151A	0.10 (±0.003)	51 (±3)	2.0 (±0.1) × 10^3
W166A	0.27 (±0.03)	3.6 (±1.1)	7.5 (±2.4) × 10^4
L407A	0.067 (±0.001)	1.2 (±0.03)	5.6 (±0.2) × 10^4
F408A	0.057 (±0.002)	5.1 (±0.9)	1.1 (±0.2) × 10^4
S117A	<0.005	nd[a]	nd[a]
H287A	<0.005	nd[a]	nd[a]
D259N	<0.005	nd[a]	nd[a]
Y44F	<0.005	nd[a]	nd[a]
S117C	0.046 (±0.004)	46 (±6)	1.0 (±0.2) × 10^3
Q55A	1.7 (±0.1)	0.75 (±0.27)	2.3 (±0.8) × 10^6
Q55E	0.55 (±0.08)	0.27 (±0.06)	2.0 (±0.5) × 10^6

[a] Not determined.

RESULTS

CocE Hydrolyzes Cocaine Faster Than Any Known Cocaine Esterase. Our kinetic experiments showed that cocE is highly proficient for cocaine hydrolysis ($k_{cat} = 7.8$ (±0.1) s^{-1}, $K_M = 640$ (±20) nM, and $k_{cat}/k_{uncat} = 5.7$ (±0.7) × 10^7) (*39*), with a specificity rate constant nearly diffusion limited ($k_{cat}/K_M = 1.2$ (±0.04) × 10^7 s^{-1} M^{-1}; $(k_{cat}/K_M)/k_{uncat} = 8.9$ (±0.4) × 10^{13} M^{-1}) (Table 2). For comparison, serum butyrylcholinesterase (BchE) catalyzes the same reaction with a specificity rate constant 10^3-fold lower ($k_{cat}/K_M = 4.6 \times 10^3$ s^{-1} M^{-1}) (*8*). CocE has both the highest k_{cat} and the lowest K_M of any enzyme known to hydrolyze cocaine (*8-12*). Furthermore, cocaethylene, a cocaine metabolite with increased in vivo toxicity and lengthened circulating half-life, is hydrolyzed by cocE with a similar rate as cocaine ($k_{cat} = 9.4$ (±0.2) s^{-1}; $K_M = 1.6$ (±0.1) μM). We did not observe any product inhibition of the cocaine hydrolysis reaction in the presence of up to 1 mM sodium benzoate or ecgonine methyl ester.

CocE Mutagenesis. A panel of 12 mutants was generated to probe contributions of residues within the acyl and alcohol specifity pockets and to validate the mechanism proposed by the crystal structure. The Michaelis−Menten parameters (k_{cat} and K_M) were measured and are summarized in Table 2. Residues that were mutated are shown in Figure 3.

Contribution of Active Site Residues toward Substrate Binding and Catalysis. The crystal structures of cocE bound to phenyl boronic acid (Figure 3) and benzoate (Figure 4) identified three residues that make extensive contacts with the acyl portion of cocaine (*26*). F261 stacks perpendicular to the benzoyl moiety of cocaine, burying 20.1 Å^2 (*40*) and making 7 van der Waals (vdw) contacts (*41*), W151 interacts with the benzoyl moiety of cocaine, burying 20.8 Å^2 and making 4 vdw contacts, and W166 π-stacks with the benzoyl moiety, burying 24 Å and making 12 vdw contacts (*26*). Additionally, the NHζ atom of W166 forms a hydrogen bond to the side chain OH of Y44 (Figure 3a). The F261A mutant

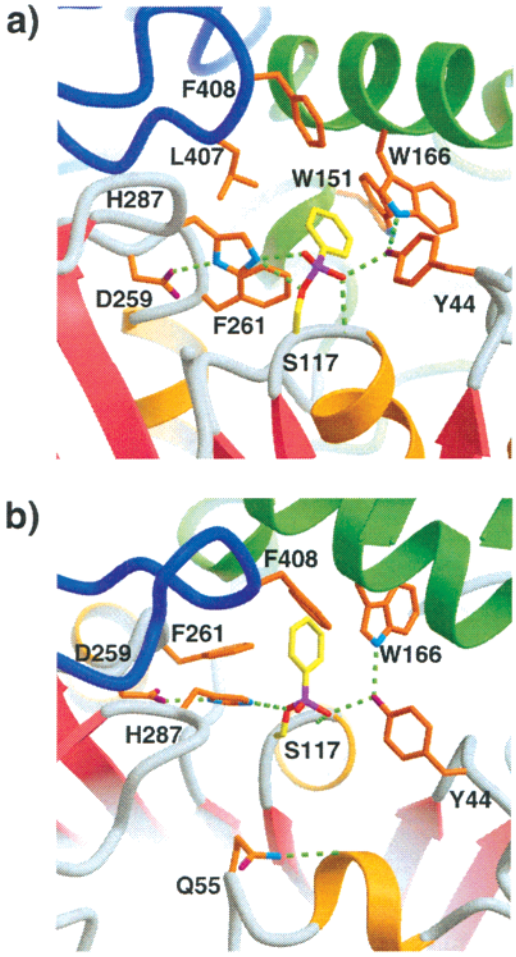

FIGURE 3: Different views of the active site of cocE bound to phenyl boronic acid. (a) (Sideview) In this view, the catalytic triad and active site residues are indicated. All three catalytic triad residues are hydrogen bonded to each other. Adapted from ref 26. (b) (Topview) In this view, the location of Q55 is indicated.

catalyzed the hydrolysis of cocaine with a 29-fold lower k_{cat} and 15-fold higher K_M. The W151A mutant catalyzed the hydrolysis of cocaine with a 78-fold lower k_{cat} and 80-fold higher K_M. Suprisingly, despite the large buried surface area and extensive number of vdw contacts between W166 and benzoate, as well as the hydrogen bond between NHζ of W166 and the side chain OH of Y44, the W166A mutant has only a 29-fold lower k_{cat}, and a 6-fold increased K_M.

Contribution of Domain 3 to Active Site Residues. The cocE crystal structure (*26*) showed extensive interactions between domain 3 (DOM3) and domains 1 and 2 (3940 Å^2 buried surface area), yet only two residues from DOM3 are located in the binding pocket (L407 and F408) (Figure 3a). These residues make only a limited number of vdw contacts with the benzoic acid (L407 = 1 vdw; F408 = 3) and the L407A and F408A mutants have only moderately increased K_M's (2-fold and 8-fold, respectively). However, each of the L407A and F408A mutations result in >100-fold decrease in k_{cat} (Table 2). Furthermore, each of these two mutants has a >10-fold lower expression level than the wild-type enzyme, and attempts to express the L407A/F408A double mutant did not result in any soluble protein. L407 and F408 form a turn in one of the loops of DOM3, which is stabilized by a hydrogen bond between the backbone NH of both L407 and F408, and the carboxylate of E161.

Catalytic Triad Residues and Y44. Mutation of any of the catalytic triad residues (S117A, H287A, D259N), as well as the oxyanion hole (Y44F), resulted in a detrimental effect on catalytic activity (>1500-fold decrease in k_{cat}) (Table 2). Due to the limitations on the sensitivity of the UV assay for rate determination, the amount of enzyme necessary to accurately measure initial rates for these four mutants would exceed the substrate concentration. Consequently, it was not possible to determine Michaelis−Menten curves for these mutants, and the reported k_{cat} values must be regarded as upper limits. Although the activity of the S117A cocE mutant was too low to be accurately measured, the S117C mutant's activity was able to be determined (k_{cat} = 0.046 s^{-1}; K_M = 46 μM). The specificity rate constant (k_{cat}/K_M) of this mutant is the lowest value of any of the mutants that could be determined, lower than the wild-type by a factor of 10^4.

S117A Crystal Structure. The crystal structure of the S117A mutant was determined at 1.76 Å resolution (Table 1) and has benzoate clearly bound in the acyl binding pocket (Figure 4b). Since these crystals were never soaked with benzoate or cocaine, benzoate must have carried through all steps of the protein purification procedure and/or been present as a contaminant in one of the purification buffers. The interaction of benzoate with the wild-type cocE (Figure 4a) buries nearly the same percentage surface area (*40*) as the interaction of benzoate with the S117A mutant (95% vs 93%, respectively), and forms a similar number of van der Waals contacts (38 mutant vs 47 wild-type) (*41*). The main difference between the two structures is the number of hydrogen bonds between the enzyme and the benzoate. In the wild-type product complex, two hydrogen bonds are donated to the benzoic acid from the Y118 backbone NH and the Y44 hydroxyl, while in the S117A mutant, a third hydrogen bond is donated from H287. The conformation of H287 in the S117A structure (Figure 4b) is nearly identical to that seen in the structure of the wild-type enzyme bound to phenyl boronic acid (Figure 3a) (*26*). The extra hydrogen bond from H287 to benzoate could provide up to 3 kcal mol^{-1} in additional stabilization for the S117A complex over the wild-type complex.

Y44F Crystal Structure. In contrast, the Y44F cocE structure, at 1.64 Å resolution (Table 1), does not have benzoate in the binding pocket, presumably due to the partial abrogation of the oxyanion hole (Figure 4c). Two water molecules were modeled and refined into relatively weak electron density in the active site. These water molecules are not within hydrogen bonding distance with each other or with any potential hydrogen bond donors/acceptors from the protein. Therefore, these two waters could collectively represent a disordered molecule of the cryo buffer, or may represent waters weakly bound in the acyl pocket. These putative water molecules do not superimpose on the region vacated by the Y44F OH. Hence, it appears that water would be relatively ineffective as a surrogate oxyanion hole in this mutant. The Y44F mutation also results in a lost hydrogen bond with NHζ of W166. There are two structural consequences of this lost hydrogen bond. First, F44 rotates 20° about χ_1 away from the binding pocket, and the side chain becomes more disordered. Second, W166 also becomes more disordered, as well as other Trp residues (W151 and W220), that form van der Waals contacts with W166. The electron density on the indole rings of W151, W166, and W220 is

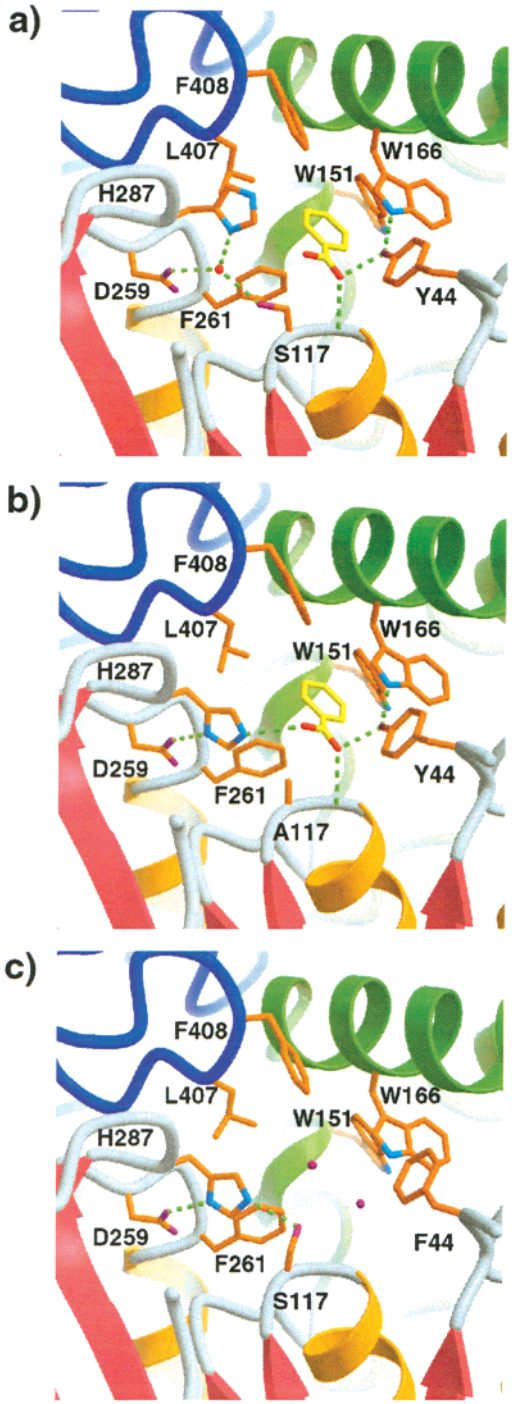

FIGURE 4: Comparison of the active site of cocE wild-type, S117A, and Y44F mutants. The view is from the same perspective as Figure 3. (a) The cocE wild-type has benzoate bound in the active site, and a single water molecule (red sphere) hydrogen bonded to the catalytic S117, H287, and D259 residues (*26*). (b) The S117A mutant of cocE also has benzoate bound, but is lacking the water molecule, causing H287 to swing down, forming hydrogen bonds to both D259 and the benzoate molecule. (c) The Y44F mutant of cocE does not have benzoate in the active site, because of the deletion of the hydrogen bond between Y44 and benzoate. In the absence of benzoate, the catalytic triad is in the productive canonical conformation for serine hydrolases. A comparison of Y44 to F44 reveals that F44 rotates 20° about χ_1 away from the binding pocket, and the side chain becomes more disordered, providing evidence for the role of W166 in orienting and stabilizing Y44 to form the oxyanion hole. Two putative water molecules (red spheres) were modeled into relatively weak electron density, and are not within hydrogen bonding distance to either each other or any potential hydrogen bond donors/acceptors from the protein.

poor compared to the native and S117A structures, as reflected by elevated *B* values.

Comparison of CocE to the Cocaine Binding Antibody GNC92H2. A comparison of the active site of cocE to the binding pocket of the cocaine binding antibody GNC92H2 (*35*) reveals a major difference in their recognition motifs. The binding pocket of GNC92H2 is negatively charged, allowing favorable interactions with the positively charged cocaine molecule, while the active site of cocE is predominantly hydrophobic. We believed that a negatively charged residue might improve the K_M of cocE through favorable interactions with the positively charged cocaine substrate, but were concerned that the negative charge on the enzyme might interact disfavorably with the negative charge on the transition state. Although a structure of cocE bound to a cocaine substrate analogue was not available, molecular modeling of cocaine into the active site, based on the benzoate-bound cocE structure (*26*), suggested that the cocaine nitrogen may lie within close proximity to residue Q55 (Figure 3b). We expressed a Q55E mutant, which introduces a negative charge into the active site. The Q55E mutant has a 2-fold lower K_M than the wild-type, but a 14-fold lower k_{cat} (Table 2). Because the effect of this mutation on the K_M was moderate, but measurable, we believed that the cocaine nitrogen could be located near Q55. To test whether the cocaine nitrogen forms a hydrogen bond to Q55, we expressed a Q55A mutant, and found that this mutant had a K_M almost identical to wild-type, and a k_{cat} that decreased by a factor of 5 ($K_M = 0.75\mu M$; $k_{cat} = 1.7\ s^{-1}$) (Table 2).

pH-Rate Profiles. To characterize the pK_a values of the residues important for catalysis, we conducted a pH rate profile of cocE for cocaine hydrolysis. Protein instability prevented the acquisition of data above pH 10.5 (Figure 5a). The pH rate profile (Figure 5b) has a maximum at pH 9.0, and was fit to a bell-shaped curve with inflection points at values of p$K_{a1} = 7.7$ (± 0.1) and p$K_{a2} = 10.4$ (± 0.1). For comparison, a graph of the pH dependence of the specificity rate constant (k_{cat}/K_M) (Figure 5c) has an additional inflection point, which results in a decrease in activity between pH 8 and 9. Since this is not observed in the plot of k_{cat} vs pH (Figure 5b), this ionizable group is important for substrate binding, but not in catalysis of the rate-determining step. Because of the partial overlap of the three titration curves in the graph of k_{cat}/K_M vs pH, we examined a plot of K_M vs pH in order to determine the apparent pK_a value of this third group. The plot of K_M vs pH for cocE (Figure 5d) indicates the presence of two titratable groups. The data below pH 10 were fit to a sigmoidal curve with a titration point of pK_{a3} = 8.4 (± 0.2), which is consistent with the third titration value in the plot of k_{cat}/K_M vs pH. Although instability of cocE above pH 10.5 prevented a mathematical determination of the value of the second inflection point, a graphical interpretation suggests a value of p$K_a = 10.4$, the same as the apparent pK_a determined from the pH rate profile (Figure 5b, p$K_{a2} = 10.4$).

Urea Unfolding. Urea denaturation of cocE was determined by both tryptophan fluorescence and circular dichroism, and the measurements show that cocE undergoes a two-transition unfolding. Tryptophan fluorescence monitors the presence of ordered/buried tryptophan residues (*38*), while circular dichroism (CD) at 222 nm monitors the α-helical

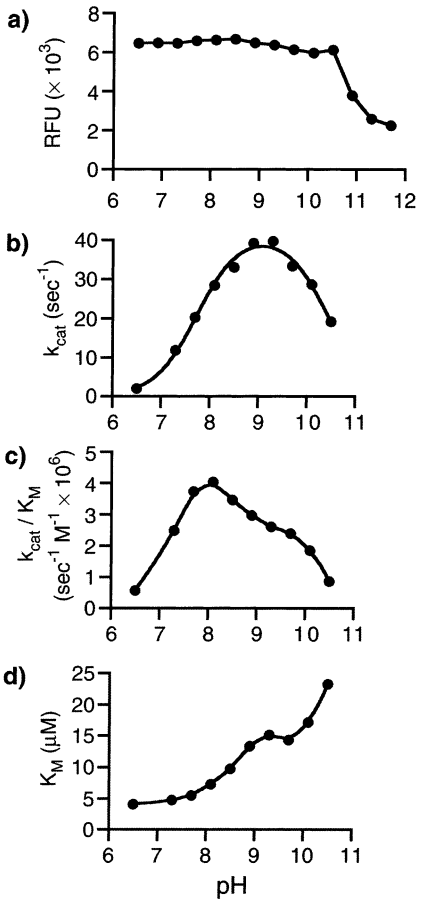

FIGURE 5: pH dependence on cocE kinetics and stability. (a) pH dependent stability of cocE measured by tryptophan fluorescence quenching(λ_{ex} = 280 nm, λ_{em} = 320 nm). CocE is stable in the pH range 6.5−10.5. (b) pH rate profile of cocE. The solid line is the best fit to equation (**1**), which indicates the titration of two groups (pK_{a1} = 7.7 (±0.1); pK_{a2} = 10.4 (±0.1)). (c) pH-dependence of k_{cat}/K_M. The asymmetric shape of the curve suggests the presence of an additional titratable group not relevant in the rate-determining step of the reaction. (d) The pH-dependence of K_M indicates the presence of two titratable groups. Fitting the data below pH 10 to a sigmoidal curve gave a value of pK_{a3} = 8.4 (±0.2). Because of enzyme instability at pH > 10.5, the pK_a of the second titratable group could not be determined. However, the data are consistent with a value of 10.4 for the second titratable group.

content of the protein (*42*). Despite these differences in detection, the measured transition values are very similar. Because DOM3 does not have any helices or Trp residues, the unfolding of DOM3 is likely not well represented using these methods, so the discussion may be restricted to DOM1 and DOM2. With fluorescence, (λ_{ex} = 280 nm; λ_{em} = 320 nm) transitions are observed at 0.5 and 3.2 M urea. Similar values for the transitions were determined by measuring molar ellipticity by CD (0.6 and 3.7 M urea) (Figure 6a). Although both techniques gave similar values for the unfolding transition points, the apparent degree of unfolding at each transition is different depending on which technique is used. Fluorescence measurements indicate that the apparent percentage of unfolding is the same for each transition, while the molar ellipticity measurements show three times more unfolding in the second transition as the first. In addition, a measurement of esterase activity shows that the first unfolding event corresponds to a complete loss of activity.

For several α/β hydrolase enzymes, DOM2 is believed to act as a flexible "lid" that can cover the active site in order

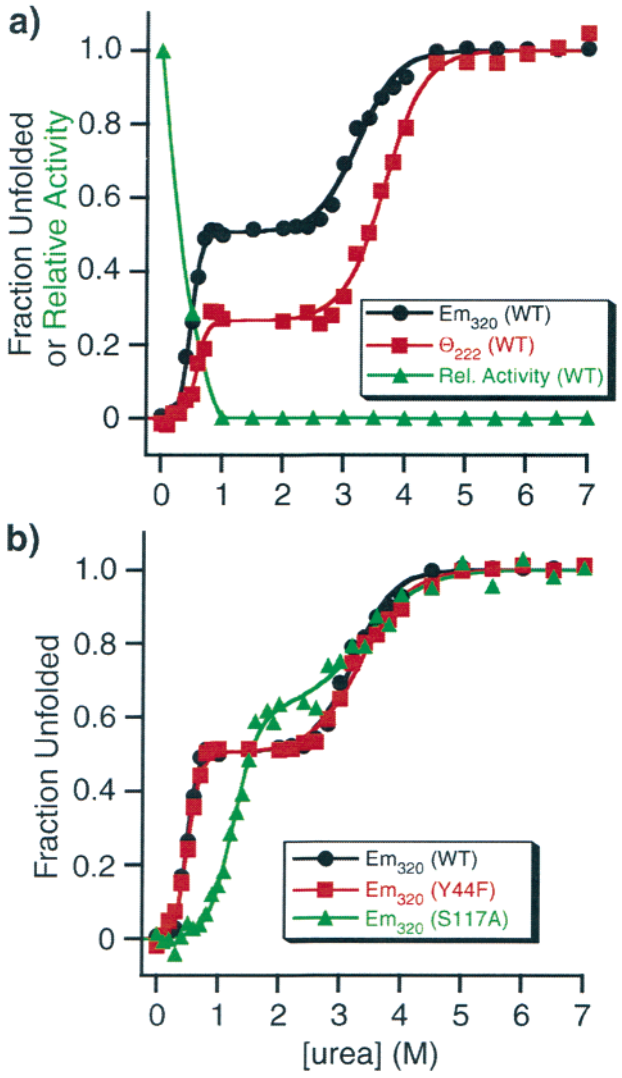

FIGURE 6: Unfolding of wild-type and mutants of cocE. (a) Comparison of urea unfolding of wild-type (WT) cocE by fluorescence (λ_{ex}=280 nm, λ_{em} = 320 nm) (black circles) and molar ellipticity (Θ_{222}) (red squares). Percent activity is also shown (green triangles). (b) Comparison of unfolding of cocE WT (black circles), cocE Y44F (red squares), and cocE S117A (green triangles). Unfolding data were fit to a double sigmoidal curve, and the activity data were plot by point-to-point interpolation.

to regulate enzyme activity and specificity (*43*). Since the size of the cocE DOM2 is one of the largest observed in the α/β hydrolase superfamily (*26*), we considered it possible that this domain could act to regulate activity and specificity, similar to the seven-bladed β-propeller fold that seals the active site of prolyl oligopeptidase (*43*). Capping of the active site of cocE by DOM2 could possibly limit product inhibition by benzoate. Inspection of the crystal structure of cocE (*26*) revealed several Trp residues (W151, W166, W220, and W235) that are buried in proximity to the active site. Because the first unfolding transition results in a loss of activity, and the helical content (θ_{222}) decreases less than the Trp fluorescence (Figure 6a), we believe the first unfolding transition corresponds to a pertubation of enzyme structure within close proximity to the active site. This pertubation could represent an unfolding or motion of DOM2 to cover the active site, or a localized unfolding of the active site itself. In contrast, the second transition would correspond to complete unfolding of the α/β cannonical fold.

To further test this putative unfolding mechanism, we measured the urea dependence on unfolding for the S117A cocE mutant. The crystal structure of this mutant revealed an additional hydrogen bond to benzoic acid from H287, compared to the wild-type structure. This additional hydrogen bond would be expected to stabilize the active site fold relative to the wild-type. If the first unfolding transition in the wild-type corresponded to unfolding of the active site, then this transition should be shifted to a higher urea concentration in the S117A mutant. Indeed, the first unfolding transition in the S117A mutant is shifted from 0.5 to 1.3 M urea compared to the wild-type, while the second transition, although broader, has a similar transition point (3.2 M vs 3.4 M) (Figure 6b). For comparison, the unfolding curve of the Y44F mutant is very similar to the wild-type, and has almost identical transition points (0.5 and 3.3 M) (Figure 6b).

DISCUSSION

CocE is the first enzyme in a metabolic pathway that allows a *Rhodococcal* strain to use cocaine as a sole carbon and nitrogen source (*25*). This strain was isolated from rhizosphere soil of the cocaine producing plant *Erythroxylum coca*, so cocE probably evolved under selection pressure for hydrolysis of cocaine. Indeed, cocE hydrolyzes cocaine with a specificity rate constant that is orders of magnitude faster than any other known cocaine hydrolyzing enzyme or catalytic antibody. The crystal structure of cocE (*26*) revealed a serine esterase of the α/β hydrolase superfamily, with a hydrophobic active site, and an oxyanion hole formed by a main chain NH and a Tyr hydroxyl. Since oxyanion holes are typically composed exclusively of backbone NH groups, cocE provides a rare opportunity to dissect the role of the oxyanion hole in catalysis through site-directed mutagenesis. These studies reveal the relative contribution of the oxyanion hole in enzyme catalysis, and, by extension, the importance of this feature in catalytic antibodies. However, there are differences in the effect of a Tyr to Phe mutation of cocE compared to prolyl oligopeptidase, which also uses a tyrosine to form the oxyanion hole motif. In addition, we compare the hydrophobic active site of cocE to the electrostatic binding pocket of the cocaine binding antibody GNC92H2. Furthermore, analysis of wild-type and mutant crystal structures of cocE show variations in the hydrogen bonding network of the active sites, which allow us to propose a model for product release. Moreover, urea denaturing studies of wild-type and structurally characterized cocE mutants allow us to probe how the mutations and corresponding changes in hydrogen bonding affects the overall stability of the enzyme.

Previously reported studies of serine hydrolases have revealed the relative contribution of residues that compose the oxyanion hole toward substrate binding and catalysis. The oxyanion hole in subtilisin BPN′ is partially formed by N155. In prolyl oligopeptidase, the oxyanion hole is partially formed by Y473. The oxyanion hole of cocE is formed by Y44, which has a lower pK_a (Y44 pK_a = 10.4) than an asparagine side chain amide (pK_a ~ 15) or main chain NH. For comparison, oxyanion pK_a's for a series of chymotrypsin and subtilisin substrate analogues have been shown to be in the range of 7−10 (*44*, *45*). Therefore, Y44 could be more efficient at stabilization of the tetrahedral intermediate than an asparagine side chain amide or a main chain NH, because proton transfer to the oxyanion is more facile (*32*). Consequently, one would expect that a Y473F mutation in prolyl oligopeptidase would have a more deleterious effect on the specificity rate constant (k_{cat}/K_M) than a N155(L/G) mutation in subtilisin BPN′. However, a N155L or N155G mutation in subtilisin BPN′ lowers k_{cat}/K_M by a factor of 150−300, while kinetic studies of a prolyl oligopeptidase Y473F mutant with the substrate *Z*-Gly-Pro-Nap show only a 8−40-fold decrease in k_{cat}/K_M (*32*). In contrast, assuming the K_M of cocE is not improved by the Y44F mutation, our measurements showed that k_{cat}/K_M decreased by at least a factor of 1500 for the Y44F mutant of cocE, which is more pronounced than the N155L or N155G mutations in subtilisin BPN′ and the Y473F mutation in prolyl oligopeptidase. The >38-fold difference in the k_{cat}/K_M ratios between the wild-type and Tyr to Phe mutants of prolyl oligopeptidase (8−40-fold) and cocE (>1500-fold) is likely because the hydrogen bond from the NH of cocE W166 to the Y44 hydroxyl both orients and activates this hydroxyl for more effective stabilization of the transition state, whereas prolyl oligopeptidase does not form a hydrogen bond from Y473 to any other residue (*46*). In addition, it has been proposed that water can form a compensating hydrogen bond in the oxyanion hole of a Y473F mutant of prolyl oligopeptidase (*32*). However the crystal structure of the Y44F mutant of cocE shows that water is relatively ineffective as a surrogate oxyanion hole. Although free energy perturbation calculations suggest that a water molecule does not move into the hole created by a N155A mutation of subtilisin (*47*), there is no direct structural information available. Therefore, as other members of this serine hydrolase class that use a Tyr in forming the oxyanion hole are identified, it will be interesting to observe any structural and kinetic effects of a Tyr to Phe mutation.

A comparison of the Y44F cocE mutant to the wild-type (Figure 4), reveals that in the Y44F mutant, F44 rotates 20° about χ_1 away from the binding pocket, and the side chain becomes more disordered. The hydrogen bond from W166 to Y44 in cocE probably results in increased transition state stabilization by cocE Y44 compared to Y473 of prolyl oligopeptidase. In fact, the disordered Trp residues (W151, W166, and W220) in the Y44F mutant suggests that they all are important for stabilizing Y44 in the correct orientation to form part of the oxyanion hole. Interestingly, in the absence of benzoate in the Y44F structure, H287 occupies the same position as in the S117A structure and the structure of the wild-type enzyme bound to phenyl boronic acid (Figure 3). In the Y44F mutant structure (Figure 4c), the NHϵ atom of H287 forms a hydrogen bond with Oγ of S117. Hence, the catalytic triad is in a productive configuration, as in the phenyl boronic acid structure (*26*). Therefore, this Y44F mutant structure may serve as a model for the native enzyme, where the catalytic triad is poised for nucleophilic attack of the scissile benzoyl ester of incoming cocaine substrate.

In addition to the Y44F mutational studies, mutation of other residues allows assessment of their relative contribution toward enzyme stability, catalysis, and substrate recognition. For example, the 170-fold reduction in k_{cat} for the S117C cocE mutant is within the range that has been observed for an active site Ser to Cys mutation in serine hydrolases. However, the K_M typically either remains unchanged or is

lowered by this mutation (*48*−*50*). For example, mutation of the catalytic Ser in subtilisin to Cys results in a 30-fold *reduction* in K_M for the hydrolysis of *p*-nitrophenyl acetate (*50*). In contrast, the S117C mutation of cocE results in a 72-fold *increase* in K_M. This shows that the active site S117 in cocE is responsible for both substrate recognition and catalysis. In contrast to the S117C mutation, which results in both a drastically lowered k_{cat} and increased K_M, mutation of either L407 or F408 to Ala decreases k_{cat} by >100-fold, but K_M values for these mutants are increased by only 2-fold and 8-fold, respectively. Furthermore, either of the L407A or F408A mutations results in a >10-fold lower expression level, This suggests that L407 and F408 are much more important for enzyme stability and activity than for substrate recognition.

For an enzymatic reaction, the pH-dependence of k_{cat} and K_M can contribute to elucidation of the catalytic mechanism, and can determine or confirm which ionizable groups are important for either substrate catalysis or binding (*31, 51, 52*). The pH rate profile of cocE was bell-shaped, with two inflection points (7.7 (±0.1) and 10.4 (±0.1), respectively). These are the apparent pK_a values of residues involved in stabilizing the transition state of the rate-determining step. Our model for the transition state is the enzyme boronic acid complex structure (*26*), which reveals a hydrogen bond between the OH of Y44 and the *Pro-S* oxygen of the phenyl boronic acid, and a hydrogen bond between Nϵ of H287 and the *Pro-R* oxygen of the phenyl boronic acid (Figure 3). We attribute the first inflection point (pK_{a1} = 7.7 (±0.1)) to ionization of the Nϵ of H287, and the second inflection point (pK_{a2} = 10.4 (±0.1)) to the pK_a of the Y44 hydroxyl. A graphical interpretation of the plot of K_M vs pH suggests the same value of 10.4 for the second inflection point. Hence, the Tyr OH hydrogen bond to benzoate and phenyl boronic acid (Figures 3 and 4a) is probably also important for substrate recognition. Because the crystal structure of cocE bound to benzoate does not reveal any other ionizable residues within the hydrophobic binding pocket that may contribute to substrate binding, we attribute the other titration point at 8.4 (±0.2) to ionization of the cocaine nitrogen, which suggests that the protonated nitrogen is recognized by the enzyme (cocaine NH pK_a = 8.5−8.6 in solution) (*53, 54*).

Although we were unsuccessful in our attempts to obtain a crystal structure of cocE bound to a cocaine analogue, we obtained very similar K_M values for the wild-type and Q55A mutant, suggesting that the cocaine nitrogen does not form a hydrogen bond to Q55. Hence, we believe the improved K_M for Q55E may be attributed to nonspecific electrostatic interaction, and not to a direct hydrogen bond. However, the inflection point on the plot of K_M vs pH suggests that the wild-type enzyme recognizes the protonated cocaine nitrogen. The lack of any other potential hydrogen bonding donors/acceptors in the hydrophobic binding pocket leaves open the possibility of the cocaine nitrogen forming a cation-π interaction with an aromatic residue (possibly Y44), much like the cation-π interaction observed in the crystal structure of the cocaine binding antibody GNC92H2 (*35*). Further structural investigations to determine the position of the cocaine nitrogen within the active site are ongoing.

Unlike the plot of K_M vs pH, there is no evidence for titration of the cocaine nitrogen in the plot of k_{cat} vs pH (Figure 5). Furthermore, cocaine and cocaethylene have very similar k_{cat} values, despite having K_M values that differ by a factor of 3 (Table 2). These observations suggest that, for cocE, like most esterases, deacylation, rather than acylation, is the rate-determining step. This illustrates one limitation in the generation of cocaine esterase antibodies. Haptens designed to mimic transition state analogues for cocaine hydrolysis typically replace the ester linkage on cocaine with a phosphonate linkage (*20*). However, the rate-determining step of serine esterases (such as cocE) is hydrolysis of the acyl-enzyme intermediate, which has a transition state that only includes the acyl portion of the ester substrate, not the alcohol moiety. Therefore, mutations which result in improved recognition of the alcohol moiety will not necessarily result in improved turnover. For example, the Q55E mutant of cocE results in an improved K_M (presumably due to favorable electrostatic interaction between E55 and the positively charged nitrogen on the alcohol moiety of cocaine), but a decrease in k_{cat}/k_M (Table 2).

The structure of cocE bound to benzoate (*26*) revealed a water molecule lodged in the active site that connects the three residues of the catalytic triad (S117, H287, D259). A search of the literature failed to identify another example of a serine hydrolase that has all three catalytic residues coordinating a single water molecule. The cocE structure bound to phenyl boronic acid lacks this water molecule, and H287 swings down to form a bifurcated hydrogen bond to both S117 Oγ and the *Pro*-R hydroxyl of phenyl boronic acid (Figure 3). The water molecule in the benzoate-bound structure (Figure 4a) prevents this latter hydrogen bond from forming, which may be a way of preventing the enzyme from binding to benzoate, limiting product inhibition by benzoate. In addition, the intervening water molecule allows the hydrogen bonding groups of the catalytic triad residues to be fulfilled. The structure of the Y44F mutant (Figure 4c) does not have benzoate bound, and also does not have the water molecule that is present in the benzoate-bound structure, providing further evidence that Y44 is important for substrate recognition in addition to formation of the oxyanion hole.

A comparison of the two published cocE wild-type structures (*26*) to the structure of the Y44F mutant, reveals that the catalytic S117 and H287 may adopt one of two possible conformations. In the published structure of cocE bound to phenyl boronic acid (Figure 3), as well as in the structure of the Y44F cocE mutant, S117 (Figure 4c) faces into the active site, and its Oγ accepts a hydrogen bond from H287 Nϵ. However, superimposing the benzoate-bound cocE structure on the Y44F and phenyl boronic acid complex structures reveals that, if S117 were to maintain its conformation in the acyl pocket immediately after deacylation, the distance between the S117Oγ and the benzoate carboxylate carbon would be close enough for steric repulsion (2.1 Å). Therefore, in the wild-type cocE structure bound to benzoate, S117 adopts a new rotamer, facing away from the active site. In this scenario, if H287 were to maintain the position seen in the Y44F and phenyl boronic acid structure, there would be additional steric repulsion between S117 and H287. Consequently, in the cocE wild-type structure bound to benzoate, H287 also adopts a new rotamer. Instead of a direct hydrogen bond between H287 and S117, there is a hydrogen bond mediated by an intervening water molecule. Impor-

tantly, this new rotamer prevents H287 from forming a hydrogen bond to benzoate. Therefore, cocE forms three hydrogen bonds to phenyl boronic acid, while forming only two hydrogen bonds to benzoate. This proposed mechanism is supported by the S117A mutant structure, where, in the absence of Ser Oγ, H287 is in the productive conformation seen in the boronic acid and Y44F structures, forming a third hydrogen bond to benzoate (Figure 4b). A consequence of this mechanism is that diffusion of benzoate from the active site allows S117, H287, and D259 to again conjoin in the productive conformation observed in the Y44F and boronic-acid-bound structures. The release of water into the bulk solution that results may provide additional driving force for product release and account for low product inhibition. The crystal structure of cocE bound to benzoate was determined from crystals that were soaked with cocaine, and the benzoate is the result of cocaine hydrolysis. Although benzoate is visible in the active site, our kinetic studies show that benzoate does not inhibit the reaction. Possibly, benzoate bound in the active site allows more facile crystallization of cocE, or the mechanism for preventing benzoate from binding in the active site is dependent on motion of active site resides that cannot take place while the enzyme is packed in a crystal lattice.

The structure of the cocaine-binding antibody, GNC92H2 (*35*) shows a very different mode of binding to cocaine than cocE. In addition to van der Waals contacts with cocaine, the immune system generated a binding pocket that incorporates a cation-π interaction and a negative charge to create high electrostatic complementarity to the positively charged tropane nitrogen. In contrast, the cocE binding pocket is relatively hydrophobic, possibly because a negatively charged specificity pocket would interact disfavorably with the negative charge acquired by the transition state in the reaction. Perhaps the most interesting difference is the overall orientation of cocaine itself in the binding pocket. In cocE, the benzoyl moiety points into the binding pocket where it is 95% buried in the specificity pocket. In the antibody structure, the benzoyl moiety points out of the binding pocket, and has fewer interactions than in cocE (33 vdw vs 43 vdw and 2 hydrogen bonds). The orientation of the benzoyl moiety is of paramount importance for eliciting effective catalytic antibodies, because the alcohol (ecgonine methyl ester) is the first leaving group, and a priori would cause severe product inhibition if buried at the bottom of the binding pocket, unable to diffuse away. As crystal structures of cocaine hydrolyzing catalytic antibodies become available, it will be interesting to see whether their active sites are hydrophobic like cocE, or negatively charged like GNC92H2.

CONCLUSIONS

The rate acceleration (k_{cat}/K_M) of cocE for cocaine hydrolysis is higher than for any other reported cocaine esterase, nearly diffusion limited. Furthermore, this enzyme hydroyzes the cocaine metabolite, cocaethylene (**4**), with a rate acceleration similar to the observed value for cocaine. No product inhibition is observed for the cocaine hydrolysis reaction at concentrations of benzoate or ecgonine methyl ester up to 1mM. Therefore, from a kinetic viewpoint, this enzyme has many qualities that are desirable for an enzyme used in a therapy for cocaine overdose. Although several esterases besides cocE, including serum butyrylcholinesterase (bChE) and human liver carboxyesterases hCE-1 and hCE-2, have been shown to hydrolyze cocaine, a comparison of k_{cat}/K_M for these enzymes shows that cocE outstrips them by at least 1000-fold. Furthermore, the lack of observable product inhibition, and the ability of cocE to accept both cocaine and cocaethylene as substrates identifies this as the first model enzyme for cocaine hydrolysis, which would be of interest for the generation of cocaine catalytic antibodies for addiction therapy. Screening small molecules for enzyme inhibition may be useful in finding leads for hapten design to elicit cocaine catalytic antibodies. Furthermore, this enzyme can serve as a positive control for novel assays to screen enzyme or catalytic antibody libraries for cocaine esterase activity.

ACKNOWLEDGMENT

We thank the Peter Wright and Jane Dyson laboratory for use of their CD spectropolarimeter, the Stanford Synchrotron Radiation Laboratory (SSRL) for support at beam lines 9-2 and 11-1, and Floyd Romesberg for helpful discussion. We also thank Benjamin List for the use of his UV plate reader.

REFERENCES

1. Kuhar, M. J. (1992) *Ciba Found. Symp. 166*, 81−95.
2. Boelsteri, U. A., and Goldin, C. (1991) *Arch. Toxicol. 65*, 351−360.
3. Hahn, I.-H., and Hoffman, R. S. (2001) *Emerg. Med. Clin. North Am. 19*, 493−511
4. Sholar, M. B., Mendelson, J. H., Mello, N. K., Siegel, A. J., Kaufman, M. J., Levin, J. M., Renshaw, P. F., and Cohen, B. M. (1998) *J. Clin. Endocrinol. Metab. 83*, 966−968.
5. Inaba, T. (1989) *Can. J. Physiol. Pharmacol. 67*, 1154−1157.
6. Jeffcoat, A. R., Perez-Reyes, M., Hill, J. M., Sadler, B. M., and Cook, C. E. (1989) *Drug Metab. Dispos. 17*, 153−159.
7. Wilkinson, P., Van Dyke, C., Jatlow, P., Barash, P., and Byck, R. (1975) *Clin. Pharmacol. Ther. 27*, 386-394.
8. Xie, W., Altamirano, C. V., Bartels, C. F., Speirs, R. J., Cashman, J. R., and Lockridge, O. (1999) *Mol. Pharmacol. 55*, 83−91.
9. Mattes, C. E., Belendiuk, G. W., Lynch, T. J., Brady, R. O., and Dretchen, K. L. (1998) *Addict. Biol. 3*, 171−188.
10. Pindel, E. V., Kedishvili, N. Y., Abraham, T. L., Brzezinski, M. R., Zhang, J., Dean, R. A., and Bosron, W. F. (1997) *J. Biol. Chem. 272*, 14769−14775.
11. Brzezinski, M. R., Spink, B. J., Dean, R. A., Berkman, C. E., Cashman, J. R., and Bosron, W. F. (1997) *Drug Metab. Dispos. 25*, 1089−1096.
12. Kamendulis, L. M., Brzezinski, M. R., Pindel, E. V., Bosron, W. F., and Dean, R. A. (1996) *J. Pharmacol. Exp. Ther. 279*, 713−717.
13. Brzezinski, M. R. (1996) *Diss. Abstr. Int. 57*, 7501−7637.
14. Boyer, C. S., and Petersen, D. R. (1992) *J. Pharmacol. Exp. Ther. 260*, 939−946.
15. Perez-Reyes, M., Jeffcoat, A. R., Myers, M., Sihler, K., and Cook, C. E. (1994) *Psychopharmacology 116*, 428−432.
16. Carroll, F. I., Howell, L. L., and Kuhar, M. J. (1999) *J. Med. Chem. 42*, 2721−2736.
17. Howell, L. L. and Wilcox, K. M. (2001) *J. Pharmacol. Exp. Ther. 298*, 1−6.
18. Ashani, Y. (2000) *Drug Dev. Res. 50*, 298−308.
19. Koetzner, L., Deng, S., Sumpter, T. L., Weisslitz, M., Abner, R. T., Landry, D. W., and Woods, J. H. (2001) *J. Pharmacol. Exp. Ther. 296*, 789−796.
20. Yang, G., Chun, J., Arakawa-Uramoto, H., Wang, X., Gawinowicz, M. A., Zhao, K., and Landry, D. W. (1996) *J. Am. Chem. Soc. 118*, 5881−5890.
21. Carrera, M. R. A., Ashley, J. A., Parsons, L. H., Wirsching, P., Koob, G. F., and Janda, K. D. (1995) *Nature, 378*, 727−730.
22. Carrera, M. R. A., Ashley, J. A., Wirsching, P., Koob, G. F., and Janda, K. D. (2001) *Proc. Natl. Acad. Sci. U.S.A. 98*, 1988−1992.

23. Carrera, M. R. A., Ashley, J. A., Zhou, B. Wirsching, P., Koob, G. F., and Janda, K. D. (2000) *Proc. Natl. Acad. Sci. U.S.A. 97*, 6202−6206.
24. Gatley, S. J. (1991) *Biochem. Pharmacol. 41*, 1249−1254.
25. Bresler, M. M., Rosser, S. J., Basran, A., and Bruce, N. C. (2000) *Appl. Environ. Microbiol. 66*, 904−908.
26. Larsen, N. A., Turner, J. M., Stevens, J., Rosser, S. J., Basran, A., Lerner, R. A., Bruce, N. C., and Wilson, I. A. (2002) *Nat. Struct. Biol. 9*, 17−21.
27. Britt, A. J., Bruce, N. C., and Lowe, C. R. (1992) *J. Bacteriol. 174*, 2087−2094.
28. Heikinheimo, P., Goldman, A., Jeffries, C., and Ollis, D. L. (1999) *Structure 7*, R141−R146.
29. Nardini, M., and Dijkstra, B. W. (1999) *Curr. Opin. Struct. Biol. 9*, 732−737.
30. Polgár, L. (1987) *New Compr. Biochem. 16*, 159−200.
31. Fülöp, V., Szeltner, Z., Renner, V., and Polgár, L. (2001) *J. Biol. Chem. 276*, 1262−1266.
32. Szeltner, Z., Renner, V., and Polgár, L. (2000) *Protein Sci. 9*, 353−360.
33. Harel, M., Kryger, G., Rosenberry, T. L., Mallender, W. D., Lewis, T., Fletcher, R. J., Guss, J. M., Silman, I., and Sussman, J. L. (2000) *Protein Sci. 9*, 1063−1072.
34. De Simone, G., Galdiero, S., Manco, G., Lang, D., Rossi, M., and Pedone, C. (2000) *J. Mol. Biol. 303*, 761−771.
35. Larsen, N. A., Zhou, B., Heine, A., Wirsching, P., Janda, K. D., and Wilson, I. A. (2001) *J. Mol. Biol. 311*, 9−15.
36. Otwinowski, Z., and Minor, W. (1997) *Methods Enzymol. 276*, 307−326.
37. Brünger, A. T., Adams, P. D., Clore, G. M., DeLano, W. L., Gros, P., Grosse-Kunstleve, R. W., Jiang, J.-S., Kuszewski, J., Nilges, M., Pannu, N. S., Read, R. J., Rice, L. M., Simonson, T., and Warren, G. L. (1998) *Acta Crystallogr. D54*, 905−921.
38. Garcia, C., Nishimura, C., Cavagnero, S., Dyson, H. J., and Wright, P. E. (2000) *Biochemistry 39*, 11227−11237.
39. The value for k_{uncat} used is from Matsushita, M., Hoffman, T. Z., Ashley, J. A., Zhou, B., Wirsching, P., and Janda, K. D. (2001) *Bioorg. Med. Chem. Lett. 11*, 87−90.
40. Connolly, M. L. (1983) *J. Appl. Crystallogr. 16*, 548−558.
41. Sheriff, S., Hendrickson, W. A., and Smith, J. L. (1987) *J. Mol. Biol. 197*, 273−296.
42. Yutani, K., Takayama, G., Goda, S., Yamagata, Y., Maki, S., Namba, K., Tsunasawa, S., and Ogasahara, K. (2000) *Biochemistry 39*, 2769−2777.
43. Nardini, M., and Dijkstra, B. W. (1999) *Curr. Opin. Struct. Biol. 9*, 732−737.
44. O'Connell, T. P., Day, R. M., Torchilin, E. V., Bachovchin, W. W., and Malthouse, J. P. G. (1997) *Biochem. J. 326*, 861−866.
45. O'Sullivan, D. B., O'Connell, T. P., Mahon, M. M., Koenig, A., Milne, J. J., Fitzpatrick, T. B., and Malthouse, J. P. G. (1999) *Biochemistry 38*, 6187−6194.
46. Fülöp, V., Böcskei, Z., and Polgár, L. (1998) *Cell 94*, 161−170.
47. Rao, S. N., Singh, U. C., Bash, P. A., and Kollman, P. A. (1987) *Nature 328*, 551−554.
48. Polgar, L., and Bender, M. L. (1967) *Biochemistry 6*, 610−620.
49. Neet, K. E., Nanci, A., and Koshland, D. E., Jr. (1968) *J. Biol. Chem. 243*, 6392−6401.
50. Neet, K. E., and Koshland, D. E., Jr. (1966) *Proc. Natl. Acad. Sci. U.S.A. 56*, 1606−1611.
51. Clark, D. D., and Ensign, S. A. (2002) *Biochemistry 41*, 2727−2740.
52. Sakurai, M., Cook, P. F., Haseman, C. A., and Uyeda, K. (2000) *Biochemistry 39*, 16238−16243.
53. Li, P., Zhao, K., Deng, S., and Landry, D. W. (1999) *Helv. Chim. Acta 82*, 85−89.
54. Nettleton, J., and Wang, G. K. (1990) *Biophys. J. 58*, 95−106.

BI026131P